液压支架用785高强度钢焊接温度场模拟与验证

迟露鑫， 孙昭藩， 伍光凤
(重庆理工大学 材料科学与工程学院，重庆 400050)

摘 要：为了优化785高强度钢焊接工艺参数，能够提供焊件上典型位置的准确热循环曲线，掌握和预测焊接过程中及焊后焊件组织、性能变化规律，采用ANSYS有限元软件对20 mm板材焊接温度场进行数值模拟，并将模拟结果与相同工艺条件下焊接试验数据进行比较. 结果表明，焊接热循环曲线的模拟结果与试验数据高度吻合；模拟焊接热影响区的宽度与实际测量值基本一致；从母材到熔合区，板条贝氏体逐渐减少，粒状贝氏体逐渐增加，晶粒尺寸也逐渐变得粗大.

关键词：785高强度钢；数值模拟；温度场；组织
中图分类号：TG 404 **文献标识码**：A **文章编号**：0253－360X(2014)08－0083－04

0 序 言

液压支架是煤矿机械化开采的核心设备，其主体部件基本上都是形状复杂的箱形焊接结构件，焊接工作量及劳动强度都很大. 目前国内外一些学者对液压支架用高强度钢已开展了焊接接头组织与性能试验研究[1-4]，为了能够提供焊件上典型位置的准确热循环曲线，精确预测焊接过程中及焊后焊件组织、性能变化规律，采用ANSYS有限元软件对20 mm板材焊接温度场进行数值模拟，并将模拟结果与相同工艺条件下焊接试验数据进行比较.

1 有限元模型的建立

1.1 试验方法

试验用母材为785高强度钢，化学成分见表1，研究对象是将两块尺寸为500 mm×300 mm×20 mm的板材沿长度方向进行对接焊，试件60°V形坡口，焊接道次具体布置见图1. 采用KRⅡ350型焊机的直流反接80% Ar + 20% CO_2气体保护焊接，根据785高强度钢等强度匹配的原则选择直径为1.6 mm的80 kg级焊丝MK·GHS80，化学成分见表2. 焊接工艺参数见表3，道次间温度控制在125 ℃.

表1 785高强度钢化学成分(质量分数，%)
Table 1 Chemical compositions of 785 steel

C	Si	Mn	S	P	Cu
0.044	0.349	1.435	0.002	0.01	0.391
N	Cr	Ni	Mo	Fe	
0.23	0.35	0.291	0.155	余量	

收稿日期：2013－01－29
基金项目：重庆高校优秀成果转化重大资助项目(KJZH11215)

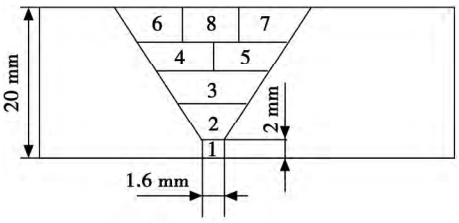

图1 焊道布置图
Fig. 1 Welding bead layout diagram

表2 MK·GHS80焊丝化学成分(质量分数，%)
Table 2 Chemical compositions of MK·GHS80

C	Si	Mn	S	P
0.09	0.58	1.8	0.01	0.013
Cu	Cr	Ni	Mo	Ti
0.22	0.42	2.91	0.52	0.12

表3 焊接工艺参数
Table 3 Welding parameters

焊道	焊接电流 I/A	电弧电压 U/V	焊接速度 v/(mm·s^{-1})	热输入 E/(kJ·cm^{-1})
1～3	230～240	29～30	4.2～4.6	24.6
4～8	360～370	30～33	5.0～5.5	24.6

1.2 有限元模型

焊接过程中的热传导是非线性关系，将785高强度钢的物理性能参数设为随温度的变化，低于熔

点时的参数值采用线性插值法处理，接近或高于熔点时采用线性外推法获得. 因此根据焊接接头在焊接过程中不同区域的温度梯度大小对模型进行区域离散，结果如图 2 所示. 焊缝区域温度梯度大，网格单元细小，热影响区和远离焊缝的母材区域温度梯度逐渐减小，网格单元则逐渐增大[5-10].

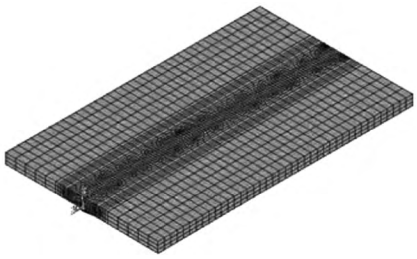

图 2 网格模型

Fig. 2 Mesh model

1.3 热源加载模型

采用体生热率的热源模型，即通过假设焊缝单元内部热生成模拟施加到节点上，生热率为

$$Q_{\mathrm{GEN}} = UI\eta/V_0 \tag{1}$$

式中: Q_{GEN} 为生热率; U 为电弧电压; I 为焊接电流; η 为热效率，在 0.80 ~ 0.90 之间; V_0 为生热单元的体积.

为了准确实现热源的动态加载，采用分段激活死单元而逐步施加热生成的方法，不仅能够精确的获得温度场分布，还便于更准确分析焊接应力场.

2 模拟结果

2.1 预热温度的计算

预热温度能够获得相对均匀的组织分布，避免或减少产生淬硬组织的倾向，还利于加速焊缝中氢的扩散逸出，防止冷裂纹的产生. 文中利用冷裂敏感指数计算最低预热温度 T_0(℃) 为

$$T_0 = 1\ 440P_{\mathrm{c}} - 392 \tag{2}$$

$$P_{\mathrm{c}} = P_{\mathrm{cm}} + \frac{w_{[\mathrm{H}]}}{60} + \frac{h}{600} \tag{3}$$

$$P_{\mathrm{cm}} = \mathrm{C} + \mathrm{Si}/30 + \mathrm{Mn}/20 + \mathrm{Cu}/20 + \mathrm{Ni}/60 + \mathrm{Cr}/20 + \mathrm{Mo}/15 + \mathrm{V}/10 + 5\mathrm{B} \tag{4}$$

式中: P_{cm} 为裂纹敏感系数; $w_{[\mathrm{H}]}$ 为熔敷金属中扩散氢含量，$w_{[\mathrm{H}]}$ = 3 mL/100 g; h 为钢板厚度; 将各个参数取值代入式中，得到 P_{cm} 为 0.19，预热温度为 49.5 ℃，显然 785 高强度钢板可在常温下采用不预热或低预热方式即可焊接.

2.2 温度场模拟结果

采用 ANSYS 有限元的生死单元技术实现热源动态加载过程，平板对接焊的温度场分布如图 3 所示.

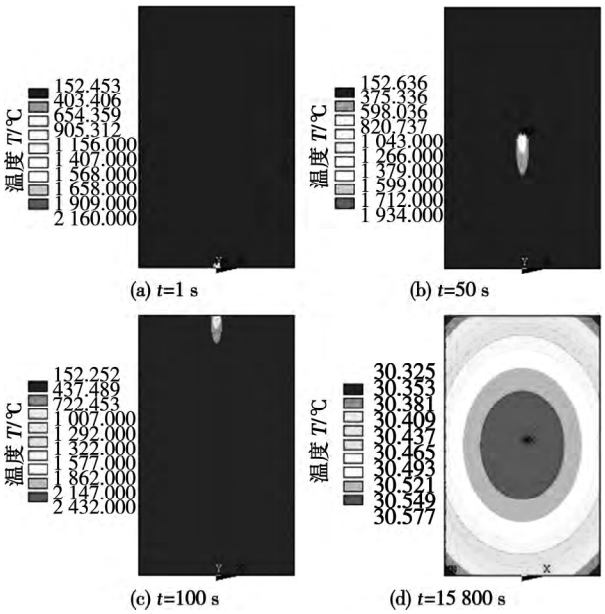

图 3 焊接接头温度分布

Fig. 3 Temperature distribution of welded joints

图 3 为最后一道焊接过程与冷却后的温度场. 图 3a 可知，焊接开始，焊接热源相当于一个固定的热源，中心温度最高 2 160 ℃，温度梯度随着到热源中心距离的增加而递减. 图 3b 是到达准稳态阶段的温度场，最高温度 1 934 ℃，并有规律的向焊接方向移动直至焊接结束. 图 3c 为最后道次焊接即将结束时的温度场，焊接收弧，温度迅速升高到 2 432 ℃，这作为焊接收弧的一个重要特点直接影响焊接应力场在焊缝末端的大小和分布. 图 3d 是平板焊接结束冷却到时间为 15 800 s 的温度场，焊接接头的温度下降到 30.577 ℃，温度梯度很小.

2.3 焊接热循环曲线分析

焊接时，母材热影响区上到焊缝不同距离的节点有不同的峰值温度，将出现不同的组织，因而也具有不同的性能. 所以准确模拟焊接热循环峰值温度的变化，避免产生局部硬化、脆化和软化等诸多组织和力学性能不均性的问题.

为了全面分析焊接热循环曲线，选择温度场特征节点的路径见图 4，在平板对接任意的位置做垂直焊缝截面 A，路径 1 是截面 A 上沿着焊缝厚度的中心线，路径 2 是平板焊缝外表面的中心线，路径 3 是在平板截面 A 上，板厚中心层垂直焊缝的位置. 三条路径上节点的焊接热循环曲线见图 5.

由图 5a，b 可知，随着热源的移动，焊缝上所有节点的热循环曲线变化趋势相似，即在热源未到达该节点前，一直保持初始温度，当热源接近该节点

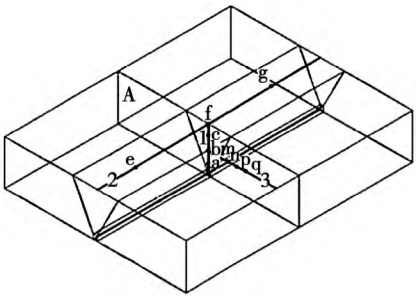

图 4　路径布置示意图

Fig. 4　Path layout diagram

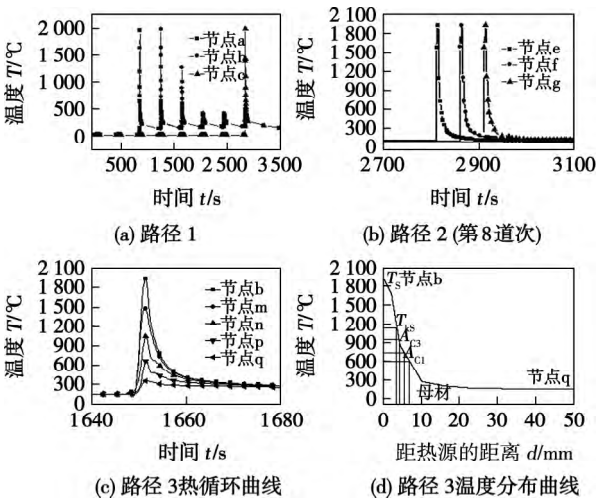

图 5　不同路径的热循环曲线

Fig. 5　Thermal circling curve of different path

检查，未发现裂纹、气孔等缺陷，因此按着温度场模拟热影响区的宽度，分析路径 3 上距离焊缝中心不同区域的组织，结果见图 6 所示.

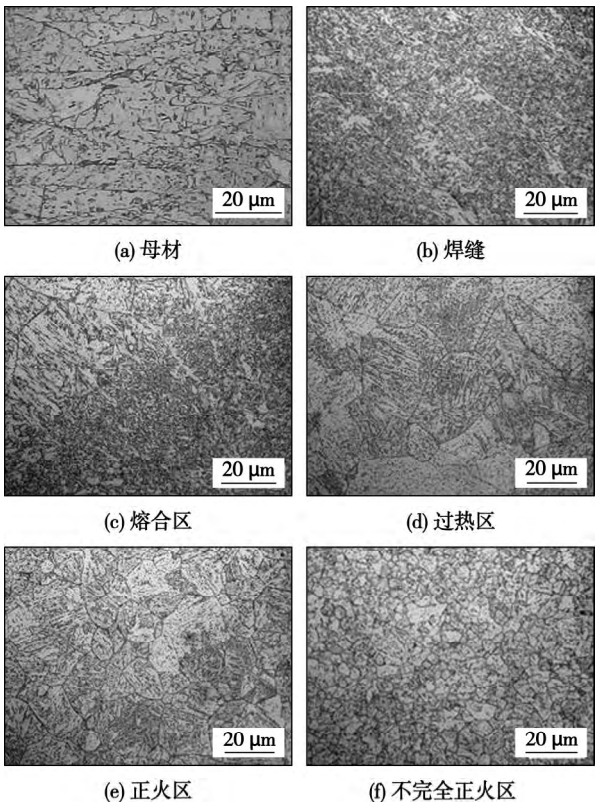

图 6　LOM 组织

Fig. 6　LOM microstructure

时，温度迅速上升到最大值后又迅速下降，温度上升的速度明显比下降的速度快. 由图 5c 可知，五个节点随着距热源距离的增大，节点达到局部最高温度的时间也逐渐延迟，其温度峰值也就逐渐减小，但节点经历的热循环曲线相似，不随位置的变化而变化. 图 5d 为路径 3 上从节点 b 到节点 q 的温度分布曲线，节点 b 为热源点，其峰值温度 1 925 ℃，节点 q 距离热源 50 mm，其峰值温度 316 ℃，结合 785 高强度钢的 A_{C_3}(925 ℃)，A_{C_1}(741 ℃) 及 SH-CCT 曲线，计算模拟热影响区的宽度为 4.019 mm，因此根据此模拟温度分布曲线可在实际焊接中方便快速地估算焊件上某些区域的峰值温度，从而预测焊接接头不同区域焊后的组织及性能，以有效地控制焊接质量.

3　试验分析与验证

3.1　金相显微组织

观察 785 高强度钢板焊接接头外观形貌，焊缝表面光滑，宽度均匀，选择在焊缝厚度 10 mm 处进行

终轧工艺使得 785 高强度钢为大量条状贝氏体和少量粒状贝氏体的混合组织，如图 6a 所示. 焊缝主要是一次相变的先共析铁素体与部分二次相变的针状铁素体的复合组织，见图 6b. 熔合区是靠近焊缝金属的过渡区域，处于粗大的过热组织前沿，由图 6c 可知，从母材出发向焊缝中心生长并深入焊缝的柱状晶，使得焊缝与母材没有明显分界线，说明焊丝与母材匹配良好，为多数的板条状贝氏体和少量粒状贝氏体. 过热区也叫粗晶区，组织与熔合区相似，是由板条状贝氏体和粒状贝氏体组成的混合组织，其原始奥氏体晶界清晰，大量的岛状和粒状的二次相在奥氏体晶粒内部沉淀析出，同时不同位向的贝氏体板条束将粗大的原始奥氏体晶粒分割，见图 6d. 由图 6e 可知，正火区组织仍然是由板条贝氏体和粒状贝氏体组成，但晶粒有明显细化，晶粒内部板条状结构只能隐约可见，粒状贝氏体的特征变得很明显，而板条状贝氏体的数量减小，岛状或粒状二次相的数量也大大减小. 接近母材的热影响区，即处于上临界和下临界温度之间的不完全正火区，为

细小贝氏体和未发生相变的贝氏体组织，见图6f. 以上分析可知，从母材到熔合区，板条贝氏体的数量逐渐减少，粒状贝氏体数量逐渐增加，同时晶粒尺寸也逐渐变粗大.

3.2 温度场模拟与试验验证

焊接热循环曲线模拟正确与否，直接影响了对焊接接头组织预测的精准性，因此为了检验模拟结果是否准确，采用WRNK-191型铠装热电偶(K型热电偶)、XSR30无纸记录仪测量第3道次和第4道次焊接过程中两个测点的实际温度，并在有限元模型对应位置上选取两个节点的热循环曲线进行对比，结果见图7.

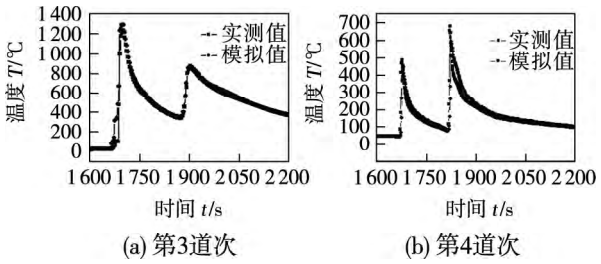

图7 热循环曲线对比

Fig. 7 Compared thermal circling curves

由图7可知，在所选择的焊接时间段内，实际测量焊件上典型位置特征点的热循环曲线与模拟结果高度吻合，虽然模拟的温度在低温时还存在少许差异，但已经对焊接组织的影响较弱，说明热模型和计算方法的正确性，可以较好预测焊接接头组织.

4 结 论

(1) 根据785高强度钢焊接温度场模拟分析可知，焊缝上所有节点经历相似的热循环曲线，不随位置的变化而变化；随着节点到热源距离的增大，其峰值温度减小，到达峰值温度的时间也逐渐延迟.

(2) 焊接实测典型位置的热循环曲线与模拟结果高度吻合，说明热模型和计算方法的正确性，可利用模拟结果快速地估算焊接接头上某些区域的峰值温度，从而预测不同区域焊后的组织及性能.

(3) 按照模拟计算焊接热影响区宽度分析785高强度钢的组织，模拟焊接热影响区的宽度与实际测量值基本一致；从母材到熔合区，板条贝氏体逐渐减少，粒状贝氏体逐渐增加，晶粒尺寸也逐渐变得粗大.

参考文献：

[1] 马成勇，田志凌，杜则裕. 热输入对800 MPa级钢焊接接头组织及性能的影响[J]. 焊接学报，2004，25(2)：23－27.
Ma Chengyong，Tian Zhiling，Du Zeyu. Effect of heat input on structure and mechanical properties of welded joint in a 800 MPa grade RPC steel [J]. Transactions of the China Welding Institution，2004，25(2)：23－27.

[2] 张优明，郑丰隆. 液压支架钢材焊接性能分析[J]. 煤矿机械，2008，29(9)：95－97.
Zhang Youming，Zheng Fenglong. Analysison welding performance of steel usedin hydraulic pressure support [J]. Coal Mine Machinery，2008，29(9)：95－97.

[3] 刘新华. 液压支架焊接接头的研究[J]. 煤矿机械，2010，31(2)：100－102.
Liu Xinhua. Study on weld joint of hydraulic power support [J]. Coal Mine Machinery，2010，31(2)：100－102.

[4] Lee H W，Kim Y H. Effect of boron contents on weldability in high strength steel [J]. Journal of Mechanical Science and Technology，2007(2)：771－777.

[5] 迟露鑫，麻永林，邢淑清，等. 压力容器用钢板焊接温度场模拟与验证[J]. 焊接学报，2012，33(5)：61－64.
Chi Luxin，Ma Yonglin，Xing Shuqing，*et al*. Test verifies and simulation on welding temperature field of steel plate for pressure vessel [J]. Transactions of the China Welding Institution，2012，33(5)：61－64.

[6] 郝永飞，陈芙蓉，杨 慧. 液压支架结构用Q550低合金高强度钢常温下的焊接[J]. 热加工工艺，2011，40(5)：169－171.
Hao Yongfei，Chen Furong，Yang Hui. Non-preheating welding process for HSLA Q550 used in hydraulic structure [J]. Hot Working Technology，2011，40(5)：169－171.

[7] 郭桂芳，陈芙蓉，李林贺. 7075铝合金电子束焊接温度场数值模拟[J]. 焊接，2006(3)：28－30.
Guo Guifang，Chen Furong，Li Linhe. Numerical simulation of temperature field of electron beam welding for 7075 aluminum alloy [J]. Welding & Joining，2006(3)：28－30.

[8] 胡美娟，刘合金，王亚军，等. 圆锥体热源模型的电子束焊接温度场数值模拟[J]. 电焊机，2005，35(7)：39－42.
Hu Meijuan，Liu Hejin，Wang Yajun，*et al*. Finite element analysis of temperature field in electron beam welding of titanium [J]. Electric Welding Machine，2005，35(7)：39－42.

[9] 徐韦锋，刘合金，朱宏强. 2219铝合金厚板搅拌摩擦焊接温度场数值模拟[J]. 焊接学报，2010，31(2)：63－66.
Xu Weifeng，Liu Hejin，Zhu Hongqiang. Numerical simulation of thermal field of friction stir welded 2219 aluminum alloy thick plate [J]. Transactions of the China Welding Institution，2010，31(2)：63－66.

[10] Gao Jiashuang，Yang Jianguo，Fang Hongyuan，*et al*. A method to simulate multilayer welding process：node dynamic relaxation method [J]. China Welding，2009，18(3)：37－41.

作者简介： 迟露鑫，女，1979年出生，博士研究生. 主要从事焊接结构质量和残余应力数值模拟方面的科研工作. 发表论文8篇.
Email：chiluxin200195@163.com

are difficult to be conducted. A unified pulsed MIG welding parameters adjusting technology based on least squares method has been proposed in this paper. The optimized fitting curve is achieved and the full advantage of the ideal data that generated in the experiments is utilized by applying a fitting relationship, which obtained through technology experiment, between the large-step welding current and other welding parameters. Besides, easier software program with simple algorithm is realized as well as a wide range of continuous adjustment of the welding parameters. Experiments are conducted after the fitting of single-pulse, double-pulse welding parameters. The experiments results indicate that the welding process is stable to obtain clear fish-scale welding seam with uniformed appearance and fewer spatters. Thus, good stability, reliability and feasibility of the proposed method are well approved.

Key words: least squares method; curve fitting; unified adjustment; digital welder

Crystal orientation in nugget zone of friction stir welded 5083 aluminum alloy plates YUAN Gecheng, LIANG Chunlang, LIU Hong, YUAN Qian (School of Materials and Energy, Guangdong University of Technology, Guangzhou 510006, China). pp 79 – 82

Abstract: The cold rolled 5083 aluminum alloy plates were welded by friction stir welding (FSW). The characteristics of grains orientation evolution in FSW nugget zone(NZ) was researched by electron backscatter diffraction(EBSD) and orientation imaging microscopy(OIM) with analyzing grain characterization, misorientation distribution, textures distribution and orientation distribution function(ODF). The results show that the dynamic recrystallization occurred in NZ due to the effect of heat and deformation which caused a severe plastic flow. Crystal in nugget zone appears to be equiaxed grain with average size 15.8 μm, and fraction of high angle grain boundaries (HAGB) appreciably increased. In the base metal, there were strong Brass texture {011} <211> and S texture {123} <634> that total fractions were above 30.6% and 13.6%, respectively. Conversely, after FSW, B and S textures in the NZ were obviously weakened as total fraction of only 4% and 1.8%, respectively. Furthermore, although the fraction of R texture {124} <211> caused by in-situ recrystallization is up to 7.7%, other common textures in face centered cubic (FCC) metal were weak in the NZ, and every fractions was also below 8%, which means that strong orientation turned into weak orientation in nugget zone.

Key words: 5083 aluminum alloy; friction stir welding; nugget zone; crystal orientation

Test verifies and simulation on welding temperature field of 785 high strength steel for hydraulic support CHI Luxin, SUN Zhaofan, WU Guangfeng (College of Materials Science and Engineering, Chongqing University of Technology, Chongqing, 400050, China). pp 83 – 86

Abstract: The as-received material was subjected to obtain thermal circling curves of typical position by ANSYS software numerical simulation in the different welding technological parameters on 20 mm thick plate to optimize welding process parameters and predict microstructures and properties for improving welding quality, compared with the simulation results and the experimental results in the same welding process conditions. It was found that the values of the thermal circling curves were close to the values measured; the simulation width of welding heat affected zone was basically the same as the measured values; the lath bainite was gradually reduced, the granular bainite increased and the grain size also became coarse from base metal to fusion zone.

Key words: 785 steel; numerical simulation; temperature field; microstructure

Humping and undercutting suppression mechanism for high speed TIG-MIG hybrid welding LOU Xiaofei[1], CHEN Maoai[1], WU Chuansong[1], YE Keli[2] (1. MOE Key Laboratory for Liquid-solid Structure Evolution and Materials processing, Institute for Materials Joining, Shandong University, Jinan 250061, China; 2. Guangxi Technological College of Machinery and Electricity, Nanning 530007, China). pp 87 – 90

Abstract: A TIG-MIG hybrid welding system was set up. A series of experiments on high speed TIG-MIG hybrid welding of low-carbon steel were launched. The effect of TIG-MIG hybrid arc characteristic, droplet transfer mode and the weld pool behavior on weld bead appearance was researched and the welding parameters were optimized. Excellent arc stability and weld appearance were obtained by setting the same value for MIG and TIG currents in the range of 240-300 A. The penetration increased and weld width decreased compared with the traditional MIG welding. Humping or undercutting were suppressed at a high welding speed up to 2.5 m/min The suppression of humping and undercutting defects in TIG-MIG hybrid welding may be attributed to the decrease in hybrid arc pressure due to the interaction between TIG and MIG arc, the disappearance of gouging region and decreases in the weld width.

Key words: TIG-MIG hybrid welding; high speed welding; humping; undercutting.

Weldablity research on the SA738Gr. B steel DING Lianzheng[1], WANG Kai[2], MENG Qingsen[1] (1. Material Science and Engineering Institute., Taiyuan University of Technology, Taiyuan 030024, China; 2. Harbin Welding Institute, China Academy of Machinery Science & Technology, Harbin 150028, China). pp 91 – 94

Abstract: The microstructure transfers were monitored by the expansion tests at the different cooling rates. By using the Gleeble-2000 thermal simulation machine, the impact toughness and the microstructures for the HAZ were also simulated. Furthermore, the weldments were performed to testify the consistency of the simulation specimen and the weldments. The results manifest that with the cooling velocity decreased, the Bainite transfer, the proeutectoid ferrite transfer, and proeutectoid ferrite pearite transfer take place in sequence. Accordingly the mechanical properties decreased. Under the condition of the multipass welds, the HAZ microstructures of the weldments consist of the mixed microstructure, but the base microstructures are same to that of the thermal simulations at the same cooing rate. The research results have a good direction and references to the welding